

Hadronic Final States*

B.R. Webber

Cavendish Laboratory, University of Cambridge,
Madingley Road, Cambridge CB3 0HE, U.K.

Abstract

The following aspects of hadronic final states in deep inelastic lepton scattering are reviewed: measuring α_s from multi-jet production rates and event shapes; alternative jet algorithms for DIS; power-suppressed corrections to event shapes; comparing jet fragmentation in e^+e^- annihilation and DIS; final states in the BFKL and CCFM formulations of small- x dynamics; exotic (instanton-induced) final states.

1. Introduction

This talk will review a selection of topics concerning hadronic final states in deep inelastic lepton scattering (DIS). One of the primary aims of studies of DIS final states is to test the predictions of QCD in more detail than is provided by measurements of the totally inclusive structure functions. By analogy with e^+e^- annihilation, it is natural to begin by studying various global measures of the jet-like properties of the final state. This is the topic of the following section. Amongst the quantities considered are the multi-jet production rates, defined according to various jet algorithms, and event shape parameter distributions. Both of these have to be defined in an infrared-safe way, so as to be insensitive to the long-distance behaviour of QCD and hence calculable in perturbation theory. Recently, it has been found that observables satisfying these conditions can still differ substantially in their sensitivity to non-perturbative physics, through the magnitude and energy dependence of corrections that are suppressed by inverse powers of a large momentum scale. Some recent theoretical ideas on

this question and their predictions for DIS will be discussed. Experimental and theoretical results on the fragmentation spectra of DIS current jets will also be reviewed.

Section 3 deals with final state features of DIS in the region of very small Bjorken x values currently being investigated at HERA. Here the theoretical analysis is more difficult and a number of basic points remain to be clarified. Some of the most promising indicators of possible new dynamics at small x concern final state properties, such as the transverse energy flow and the production of forward jets with transverse momenta comparable to the DIS momentum transfer Q .

In section 4, a more speculative but exciting possibility for DIS final states is discussed, namely non-perturbative processes that might be induced by QCD instantons. The associated final states would have high hadron multiplicities without any prominent multi-jet production.

Section 5 contains some concluding remarks.

2. Jet Physics

2.1. Jet rates

Multi-jet production rates are at present the only features of DIS final states that have been fully predicted to next-to-leading order in QCD perturbation theory [1].

* Plenary talk at the Workshop on Deep Inelastic Scattering and QCD, Paris, April 1995. Research supported in part by the UK Particle Physics and Astronomy Research Council and by the EC Programme "Human Capital and Mobility", Network "Physics at High Energy Colliders", contract CHRX-CT93-0357 (DG 12 COMA).

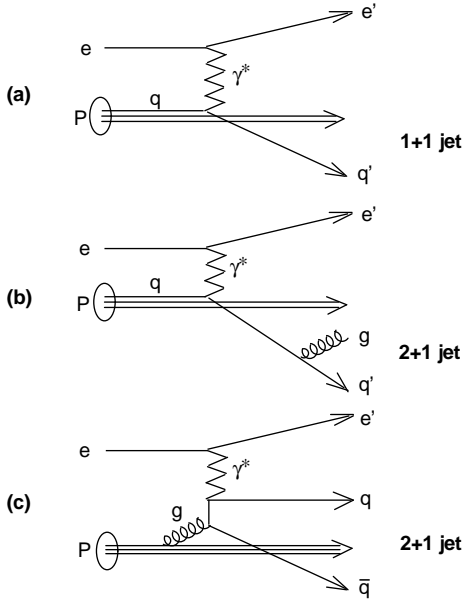


Figure 1. Typical diagrams for neutral current deep-inelastic scattering: (a) Born term, (b) QCD Compton scattering, (c) boson-gluon fusion.

Denoting by $\sigma_{n+1}(x, Q^2; y_{\text{cut}})$ the cross section for the production of n jets plus the remnant jet, at given values of Bjorken x , momentum transfer-squared Q^2 and jet resolution y_{cut} , we have schematically

$$\sigma_{n+1}(x, Q^2; y_{\text{cut}}) = \alpha_s^{n-1}(Q) A_n(x, Q^2; y_{\text{cut}}) + \alpha_s^n(Q) B_n(x, Q^2; y_{\text{cut}}) + \dots \quad (1)$$

where A_n and B_n are calculable in terms of the parton distribution functions of the proton. The leading terms A_n are given by the corresponding tree graphs as illustrated in figure 1. Once the next-to-leading term B_n is known for $n > 1$, this provides a method for measuring the strong coupling α_s .

There are several different ways of defining jets, with correspondingly different definitions of the jet resolution y_{cut} . So far, the next-to-leading function B_2 for 2+1 jets has been computed only for the *modified JADE* jet clustering algorithm [1, 2]. Here one defines for each pair of particles or clusters i and j the quantity

$$y_{ij} = 2E_i E_j (1 - \cos \theta_{ij})/W^2 \simeq m_{ij}^2/W^2 \quad (2)$$

where m_{ij} is the invariant mass of the pair and W is the overall hadronic centre-of-mass energy ($W^2 = Q^2(1-x)/x$). The pair with the smallest value of y_{ij} are clustered, the process being repeated until all y_{ij} 's are above y_{cut} . The proton remnant is included in the clustering procedure as a ‘pseudoparticle’ carrying any missing longitudinal momentum that is lost down the beam pipe. After clustering, the clusters remaining at

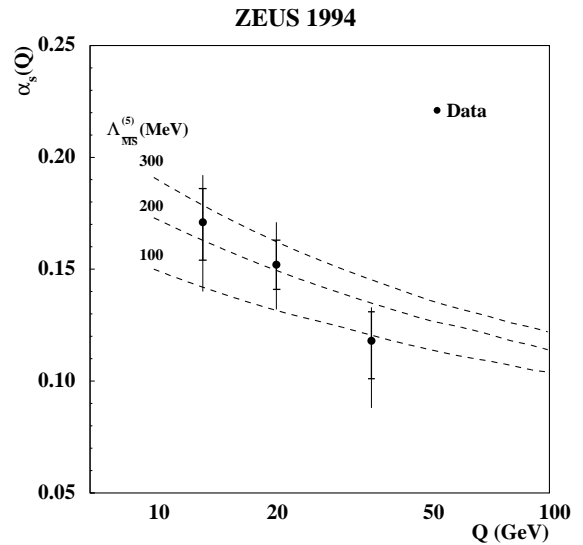


Figure 2. Results from the ZEUS collaboration on α_s for different Q^2 regions.

resolution y_{cut} are defined as jets, the one containing the pseudoparticle being the remnant jet.

Using the above jet definition at $y_{\text{cut}} = 0.02$, the HERA experiments have obtained evidence of the running of α_s , and have measured its value as [3, 4]

$$\alpha_s(M_Z) = 0.123 \pm 0.018 \quad (\text{H1}), \quad (3)$$

$$\alpha_s(M_Z) = 0.117 \pm 0.005^{+0.004}_{-0.005} \pm 0.007 \quad (\text{ZEUS}), \quad (4)$$

where the three components of the error in (4) are statistical, experimental systematic and theoretical systematic, respectively. In figure 2, for example, the ZEUS results on α_s as a function of Q^2 are shown, together with the expected behaviour for various values of the 5-flavour $\overline{\text{MS}}$ QCD scale $\Lambda_{\overline{\text{MS}}}^{(5)}$. The inner error bars show the statistical errors only, while the outer ones represent statistical and systematic errors added in quadrature.

In addition to the modified JADE algorithm used in the above analyses, there are other possible jet definitions, which have some theoretical advantages but are not yet predicted to $\mathcal{O}(\alpha_s^2)$. For future reference I mention here the *factorizable JADE* algorithm [5], with

$$y_{ij} = 2E_i E_j (1 - \cos \theta_{ij})/Q^2 \simeq m_{ij}^2/Q^2, \quad (5)$$

i.e. differing from (2) only in the normalization, and the k_{\perp} -algorithm for DIS [6], in which

$$y_{ij} = 2 \min\{E_i^2, E_j^2\} (1 - \cos \theta_{ij})/Q^2 \simeq k_{\perp ij}^2/Q^2, \quad (6)$$

where k_{\perp} represent the transverse momentum of i relative to j , or vice versa, whichever is the smaller. In

both these algorithms the definition of the remnant jet is also different from that in the modified JADE algorithm: instead of the pseudoparticle, one introduces a fixed momentum vector $p_r = xp$, where p is the incoming proton momentum, and computes y_{ir} , obtained by clustering p_i with p_r , along with y_{ij} at each stage. If the smallest of all these is y_{kr} , then k is classified as part of the remnant jet and is not available for further clustering.

A substantial part of the theoretical systematic error in the α_s determinations (3) and (4) is associated with *hadronization corrections*, i.e. the non-perturbative corrections applied to the perturbative predictions before comparing them with hadron-level data. The k_\perp -algorithm in particular may have some advantages in reducing this source of error. As we shall see in section 2.3, there are theoretical indications that non-perturbative effects should be smaller for algorithms based on the k_\perp -resolution variable (6) rather than the JADE resolution (2) or (5).

2.2. Event shapes

Shape variables that describe the “jettiness” of the final state have proved useful in e^+e^- annihilation studies; one of the earliest and still most commonly-used is the *thrust*, T , defined as [7]

$$T = \max \frac{\sum_i |\vec{p}_i \cdot \vec{n}|}{\sum_i |\vec{p}_i|} \quad (7)$$

where the sum is over all final-state particles and the maximum is with respect to the direction of the unit vector \vec{n} . The thrust has value one-half for a fully isotropic final state, and its value approaches unity as the configuration in the hadronic centre-of-mass frame becomes more two-jet-like.

If the definition (7) is taken over directly to describe DIS, the value of the thrust is strongly affected by the properties of the proton remnant. This is not very satisfactory since the remnant is not involved in the hard scattering and in any case is often not seen in the detector. An alternative definition involves looking at the final state in the *Breit frame* of reference instead of the hadronic c.m. frame. The Breit frame is the one in which the momentum transfer from the lepton is purely spacelike and lies along the z -axis: say, $q^\mu = (0, 0, 0, Q)$. In this frame the current jet is usually in the same hemisphere as q^μ (the current hemisphere), while the remnant jet is in the opposite (remnant) hemisphere. We may therefore define the “current jet thrust” T_c as $2P/Q$ where P is the total longitudinal momentum in the current hemisphere in the Breit frame.

The distribution of the current jet thrust has not yet been calculated to next-to-leading order. A calculation and experimental measurements of this quantity would

be valuable for α_s determination and for comparison with e^+e^- results. We shall see in the following subsection that recent ideas about non-perturbative contributions could be tested by such a comparison.

One shape variable whose distribution can already be predicted to next-to-leading order is y_{2+1} , the value of the jet resolution y_{cut} at which two jets plus the remnant jet can just be resolved in the final state. This distribution is essentially just the derivative of the $1+1$ -jet rate with respect to y_{cut} , which can be deduced (for the modified JADE jet algorithm) from the jet rate calculations described above. So far, the data have not been presented in this form. Again, we shall see below that ideas about non-perturbative contributions could be tested using this quantity, by studying the Q^2 -dependence of the discrepancy between the perturbative prediction and experiment.

2.3. $1/Q$ corrections

A field of recent theoretical activity that needs more experimental input, which could be provided by studies of final states in DIS, involves the investigation of $1/Q$ corrections to hadronic event shapes [8, 9, 10, 11, 12, 13, 14, 15, 16].

In e^+e^- annihilation, it is well known that many event shape variables receive significant non-perturbative contributions of the form λ/Q , where λ is typically of the order of 1 GeV and Q is the hard process scale, which in e^+e^- annihilation is the centre-of-mass energy, $Q = E_{\text{cm}}$. This is seen for example in the mean value of the thrust (figure 3): the discrepancy between the data and the perturbative prediction (dashed) shows a clear $1/E_{\text{cm}}$ dependence. As also illustrated in figure 3, the full dependence on E_{cm} is well described by the Monte Carlo event generators JETSET [17] and HERWIG [18]. The discrepancy has therefore customarily been described as a “hadronization correction”, estimated according the the models of the hadronization process that are built into those programs. Similar corrections, also with a $1/Q$ dependence, are found in differential event shape distributions.

Recent theoretical studies suggest that $1/Q$ corrections are not necessarily related to hadronization, but may instead be a universal soft gluon phenomenon associated with the behaviour of the running coupling at small momentum scales [11, 12]. The term ‘universal’ means that they could be expressible in terms of a few non-perturbative parameters that are not themselves calculable but have calculable process-dependent coefficients.

Final states in deep inelastic scattering are an excellent place to test these ideas experimentally. If the conjectured universality is true, there should be $1/Q$

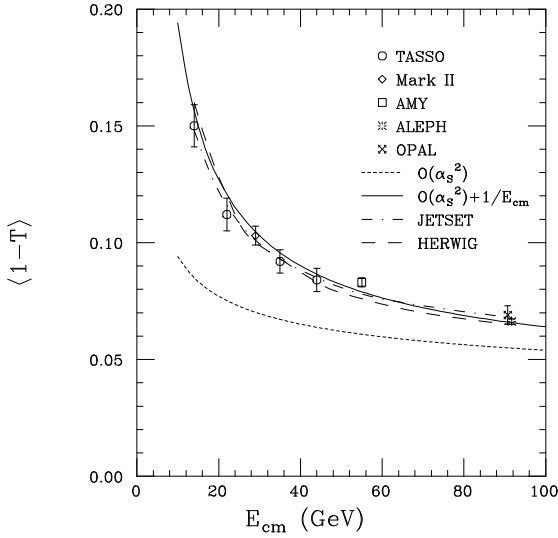


Figure 3. Mean value of $1 - T$ in e^+e^- annihilation.

corrections to shape variables for DIS final states, where Q is now the usual DIS momentum transfer variable. Furthermore the coefficients of $1/Q$ should be related to those measured in e^+e^- annihilation [16].

From the experimental point of view, DIS appears to be a good process in which to study $1/Q$ effects, since the wide range of Q^2 values available in a single experiment should make it straightforward to disentangle the relevant power-behaved terms from the logarithmically-varying perturbative terms. Note also that the terms in question are dominant over the more familiar higher-twist corrections, which behave like $1/Q^2$.

Before giving some illustrative predictions for DIS final states, let us recall the mechanism proposed in ref. [11] as the source of $1/Q$ corrections. For definiteness, consider again the mean value of the thrust in e^+e^- annihilation. The “improved” leading-order perturbative prediction of this quantity is of the form

$$\langle 1 - T \rangle \sim \int_0^Q dk_\perp \alpha_s(k_\perp) f_T(k_\perp, Q). \quad (8)$$

By “improved” we mean that in the perturbative prediction we use the running coupling constant evaluated at a scale given by the transverse momentum k_\perp of the emitted final-state gluon [19]. The function f_T turns out to have the behaviour

$$f_T(k_\perp, Q) \simeq 4C_F/\pi Q \quad \text{for } k_\perp \ll Q. \quad (9)$$

Substituting this and the perturbative expansion for

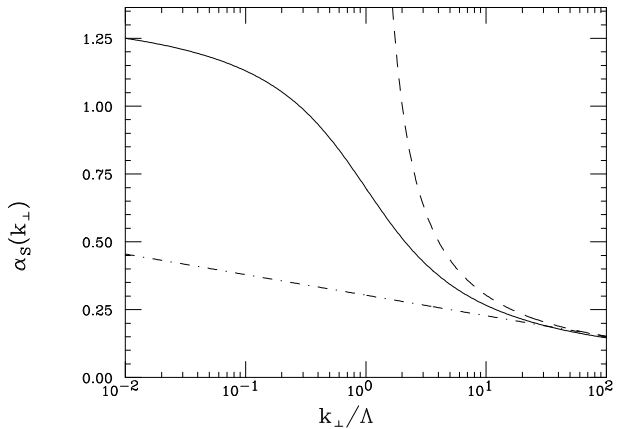


Figure 4. Solid curve: possible infrared-finite behaviour of the strong coupling at low scales. Dashed: one-loop running $\alpha_s(k_\perp)$. Dot-dashed: expansion of one-loop $\alpha_s(k_\perp)$ to second order in $\alpha_s(Q)$ for $Q/\Lambda = 100$.

$\alpha_s(k_\perp)$,

$$\alpha_s^{\text{pert}}(k_\perp) = \alpha_s(Q) + b \ln \left(\frac{Q}{k_\perp} \right) \alpha_s^2(Q) + \dots \quad (10)$$

($b = [33 - 2N_f]/6\pi$) into eq. (8), we find

$$\langle 1 - T \rangle \sim \frac{4C_F}{\pi} \alpha_s(Q) \sum_n n! [b \alpha_s(Q)]^n. \quad (11)$$

Because of the $n!$ in the coefficient, the series is strongly divergent. Therefore by “improving” the perturbative prediction we have made it meaningless!

The reason for the divergence is that the perturbative expression for $\alpha_s(k_\perp)$ diverges at the Landau pole, $k_\perp = \Lambda$. Therefore, if we use α_s^{pert} in eq. (8), the integral is not well defined. On the other hand if we truncate the series (10) at any finite n there is only an integrable divergence at $k_\perp = 0$. Consequently, for consistency, the series must diverge.

One can attempt to give a meaning to the integral involving α_s^{pert} by specifying how to deal with the Landau pole. The various options differ by terms of order $1/Q$ and therefore one is led to expect a term of this form in the true answer, whose coefficient cannot be determined within perturbation theory. This is an example of the (infrared) *renormalon ambiguity* [9, 13, 14, 20].

In ref. [11] a more phenomenological approach is proposed. Suppose that a meaningful, universal form of

$\alpha_s(k_\perp)$ can be defined for all values of k_\perp ; for example, the solid curve in figure 4. Then the integral

$$\int_0^\mu dk_\perp \alpha_s(k_\perp) \equiv \mu \bar{\alpha}_0(\mu) \quad (12)$$

exists for all $\mu \geq 0$. For μ sufficiently large ($\mu \gg \Lambda$) we have $\alpha_s(k_\perp) \simeq \alpha_s^{\text{pert}}(k_\perp)$ for $k_\perp > \mu$. Therefore we may write

$$\langle 1 - T \rangle \simeq \langle 1 - T \rangle^{\text{pert}} + \langle 1 - T \rangle^{\text{pow}} \quad (13)$$

where $\langle 1 - T \rangle^{\text{pert}}$ represents the second-order perturbative prediction, while (for $\Lambda \ll \mu \ll Q$)

$$\begin{aligned} \langle 1 - T \rangle^{\text{pow}} &= \frac{4C_F}{\pi Q} \int_0^\mu dk_\perp \left[\alpha_s(k_\perp) \right. \\ &\quad \left. - \alpha_s(Q) - b \ln \left(\frac{Q}{k_\perp} \right) \alpha_s^2(Q) \right] \\ &= -\frac{4C_F \mu}{\pi Q} \left[\bar{\alpha}_0(\mu) - \alpha_s(Q) \right. \\ &\quad \left. - b \left(\ln \frac{Q}{\mu} + 1 \right) \alpha_s^2(Q) \right]. \quad (14) \end{aligned}$$

The negative terms in the integrand express the fact that we have subtracted the perturbative contribution from $k_\perp < \mu$ and replaced it by the non-perturbative expression (12). As shown in figure 4, the subtracted part is probably smaller than $\alpha_s(k_\perp)$ and therefore we expect a positive power correction. Good agreement with the thrust data shown in figure 3 is found for $\bar{\alpha}_0(2 \text{ GeV}) = 0.52 \pm 0.04$ [11].

Using the same approach, one finds power corrections like (14) for a wide range of final-state observables in hard processes, including deep inelastic scattering [15, 16]. In general the correction is of the form[†]

$$\begin{aligned} F^{\text{pow}} &= a \frac{4C_i}{\pi r} \left(\frac{\mu}{Q} \right)^r \log^s \left(\frac{Q}{\mu} \right) \left[\bar{\alpha}_{r-1}(\mu) \right. \\ &\quad \left. - \alpha_s(Q) - b \left(\ln \frac{Q}{\mu} + \frac{1}{r} \right) \alpha_s^2(Q) \right] \quad (15) \end{aligned}$$

where a , r and s ($s = 0$ or 1) are constants that depend on the observable F , C_i is the relevant colour factor ($C_i = C_F = 4/3$ for the quantities we are considering) and

$$\bar{\alpha}_{r-1}(\mu) \equiv r \mu^{-r} \int_0^\mu dk_\perp k_\perp^{r-1} \alpha_s(k_\perp). \quad (16)$$

Predictions for the coefficient a and the exponents r and s for various e^+e^- , deep inelastic and Drell-Yan observables are listed in table 1 [16].

[†] In ref. [11] there is a constant added to the final $1/r$, corresponding to the use of a different renormalization scheme for the definition of $\bar{\alpha}_{r-1}$.

F	a	r	s
$\langle T \rangle_{\text{ee}}$	-1	1	0
$\langle C \rangle_{\text{ee}}$	$3\pi/2$	1	0
$(\sigma_L/\sigma_{\text{tot}})_{\text{ee}}$	$\pi/4$	1	0
$\langle M_j^2/Q^2 \rangle_{\text{ee}}$	1	1	0
$\langle B \rangle_{\text{ee}}$	1	1	1
$\langle y_3 \rangle_{\text{ee}}^{\text{J}}$	1	1	0
$\langle y_3 \rangle_{\text{ee}}^{k_\perp}$	-	2	-
<hr/>			
$\langle T_c \rangle_{\text{DIS}}$	-1	1	0
$\langle y_{2+1} \rangle_{\text{DIS}}^{\text{mJ}}$	$\sqrt{\frac{x}{1-x}}$	1	0
$\langle y_{2+1} \rangle_{\text{DIS}}^{\text{fJ}}$	1	1	0
$\langle y_{2+1} \rangle_{\text{DIS}}^{k_\perp}$	-	2	-
<hr/>			
$\langle q_t/Q \rangle_{\text{DY}}$	1	1	1
$\langle q_t^2/Q^2 \rangle_{\text{DY}}$	-	2	-

Table 1. Predictions for power corrections to e^+e^- , deep inelastic and Drell-Yan observables.

The e^+e^- quantities T , C and σ_L are the thrust, C -parameter and longitudinal cross section, discussed in ref. [11]. M_j^2 represents the jet mass-squared. In one-loop order this may correspond to the heavy jet mass-squared M_h^2 or the heavy-light jet difference $M_h^2 - M_l^2$, there being no difference between these quantities until multi-jet contributions become significant. Discrepancies between the coefficients of $1/Q$ corrections to these quantities therefore measure the non-perturbative effect of multi-jet contributions not associated with the running of α_s [13]. In our treatment the effective expansion parameter here is $\bar{\alpha}_0 \sim 0.5$, and so the predicted coefficients would not be expected to be more reliable than about $\pm 50\%$. Similarly for B , which represents either the total or wide jet broadening [21] at one-loop order.

Quantities like $\langle B \rangle_{\text{ee}}$ have enhanced ($s = 1$) leading power corrections associated with the logarithmically growing phase space for gluon emission with limited k_\perp . Such quantities also have non-enhanced terms with the same power, but these are more difficult to predict because they receive contributions from the non-soft, wide-angle region.

The quantities $\langle y_3 \rangle_{\text{ee}}^{\text{J}}$ and $\langle y_3 \rangle_{\text{ee}}^{k_\perp}$ are the values of the jet resolution y_{cut} at which three jets are just

resolvable, using the JADE and k_\perp -algorithms. The k_\perp -algorithm is “better” in that its correction is suppressed by one extra power of Q . This could be related to the observation that this algorithm has smaller hadronization corrections.

Note that predictions for the coefficient a and the logarithmic exponent s are not shown in table 1 for observables which, like $\langle y_3 \rangle_{ee}^{k_\perp}$, have no $1/Q$ correction. When the leading power correction is of order $1/Q^2$, there are other mechanisms that can give contributions of the same order, making the predictions less straightforward [14, 15].

Turning to the observables for deep inelastic scattering, we consider first the current jet thrust as defined previously. For this quantity the power correction (unlike the perturbative contribution) is predicted to be approximately equal to that for the thrust in e^+e^- annihilation at $E_{cm} = Q$, independent of Bjorken x . As discussed above, corrections to this relationship are higher-order in $\bar{\alpha}_0$, and so the equality should be good to about $\pm 50\%$.

The observable $\langle y_{2+1} \rangle_{DIS}^A$ is the mean jet resolution at which two jets plus the remnant jet are just resolvable in DIS using jet clustering algorithm A. We denote by $A = mJ$, fJ and k_\perp the modified and factorizable JADE and k_\perp algorithms defined above. The mJ algorithm is the only one for which next-to-leading order predictions are available at present [1]. Note that in this case the factor of $\sqrt{x/(1-x)}$ in the coefficient a means that the power correction should be approximately the same as that in e^+e^- annihilation at $E_{cm} = W = Q\sqrt{(1-x)/x}$, rather than at $E_{cm} = Q$.

In the factorizable JADE-type algorithm (fJ), on the other hand, the scale of the power correction is Q instead of W , making it larger than that for the modified JADE algorithm. One should remember, however, that this is also true of the perturbative terms, so the relative correction is similar.

As in e^+e^- annihilation, the k_\perp -type algorithm for DIS [6] has a smaller (order $1/Q^2$) correction, suggesting a smaller “hadronization” correction.

For Drell-Yan processes, q_t in table 1 is the transverse momentum of the lepton pair and Q is its invariant mass. The mean value of q_t/Q is expected to have a $1/Q$ correction, again log-enhanced due to the growing phase space for gluon emission. The possibility of a $1/Q$ power correction to the Drell-Yan cross section itself has also been considered [9] but seems less likely [14, 15].

2.4. Fragmentation studies

In addition to jet rates and event shapes, one can investigate the fragmentation properties of jets in DIS final states [22, 23]. Here again it is advantageous

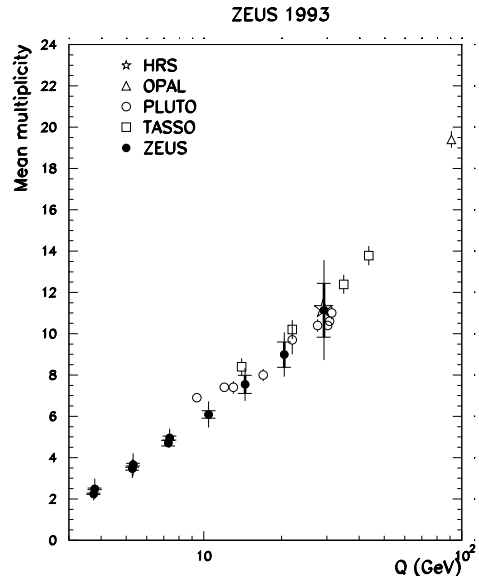


Figure 5. Mean charged multiplicity in e^+e^- (open symbols) and DIS final states.

to study the current hemisphere in the Breit frame, which should be comparable to a single hemisphere of an e^+e^- final state at $E_{cm} = Q$. In particular the average multiplicity of charged hadrons should be asymptotically independent of Bjorken x , with a Q^2 -dependence given by the next-to-leading-logarithmic (NLL) prediction [24]

$$\langle n_{ch} \rangle \sim A \alpha_s^b(Q) \exp[c/\sqrt{\alpha_s(Q)}], \quad (17)$$

where the normalization A is not predicted (but should be equal to that for a single e^+e^- hemisphere) while the exponents b and c are known constants. As shown in figure 5, the data on charged multiplicity in current fragmentation do follow the Q -dependence of the e^+e^- data, which in fact agree well with the QCD prediction (17).

One can go on to compare other properties of the charged multiplicity distribution in current jet fragmentation with the corresponding results for a single hemisphere in e^+e^- annihilation. For example, the second binomial moment $\langle n_{ch}(n_{ch} - 1) \rangle$ should satisfy the x -independent relation [25]

$$\frac{\langle n_{ch}(n_{ch} - 1) \rangle}{\langle n_{ch} \rangle^2} \sim \frac{7}{4} - \left(\frac{55}{8} - \frac{5}{81} N_f \right) A \sqrt{\frac{\alpha_s(Q)}{6\pi}} + \mathcal{O}[\alpha_s(Q)]. \quad (18)$$

The data show that the shape of the distribution does appear to depend on Q^2 and not explicitly on x , but a comparison with eq. (18) has not yet been presented.

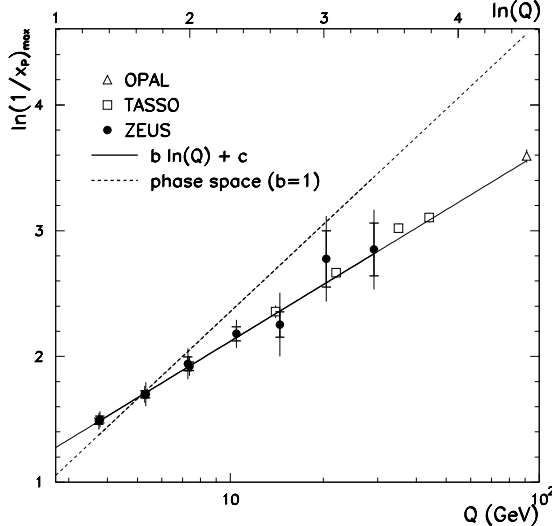


Figure 6. Position of the peak in the $\ln(1/x_p)$ distribution for e^+e^- (open symbols) and DIS final states.

Studies of the current jet fragmentation function, i.e. the inclusive single particle momentum distribution, are also being performed [22, 23]. One expects that the distribution of the logarithm of the momentum fraction, $\xi = \ln(1/x_p)$, where $x_p = 2p/Q$ in the Breit frame current hemisphere, should be the same as that in e^+e^- annihilation at $E_{\text{cm}} = Q$. The distribution in ξ should be approximately Gaussian, with a peak that moves linearly with $\ln Q$. More precisely, to NLL accuracy we expect the peak to be at $\xi = \xi^*$ where

$$\xi^* \sim \frac{1}{2} \ln \left(\frac{Q}{\Lambda_{\text{eff}}} \right) \left[1 + \left(\frac{11}{2} - \frac{1}{27} N_f \right) \sqrt{\frac{\alpha_s(Q)}{6\pi}} + \dots \right]. \quad (19)$$

Here Λ_{eff} is an effective scale (not necessarily equal to $\Lambda_{\overline{\text{MS}}}^{(5)}$) and the ellipsis represents $\mathcal{O}[\alpha_s(Q)]$ corrections. As shown in figure 6, a linear leading $\ln Q$ dependence is seen, in good agreement with the e^+e^- data and in disagreement with a simple phase space model.

Again, it will be interesting to test other QCD predictions concerning the form of the ξ -distribution. For example, the NLL result for the r.m.s. width σ is [26]

$$\sigma^2 \sim \frac{1}{36} \ln \left(\frac{Q}{\Lambda_{\text{eff}}} \right) \left[\sqrt{\frac{6\pi}{\alpha_s(Q)}} - \frac{33}{8} + \frac{1}{4} N_f + \dots \right]. \quad (20)$$

As the data become more precise, it will be necessary to go beyond the NLL treatment, and systematic differences between e^+e^- and DIS jet fragmentation should become manifest, due to the different higher-

order corrections, quark flavour composition and threshold effects in the two processes.

3. Small x Final States

3.1. Theoretical remarks

One of the areas of greatest current interest in DIS physics is QCD dynamics in the region of small Bjorken x . Although HERA has opened up a much larger window on the small- x region, it is still the case at present that different theoretical approaches can account for the increase in the totally inclusive structure function F_2 at small x [27]. It is therefore important to consider less inclusive aspects of DIS, and in particular to identify features of the final state that might distinguish between the different mechanism proposed for the small- x rise in F_2 .

Outside the small- x region, the standard approach embodied in the DGLAP Q^2 -evolution equations [28] has a firm theoretical basis in the operator product expansion, renormalization group and factorization theorems. A simple extrapolation of DGLAP evolution to small x still appears to be consistent with the structure function data. The corresponding final states are dominated by strongly ordered configurations of transverse momentum k_t and virtuality k^2 along the ladder of partons connecting the soft, low-virtuality proton constituents to the hard subprocess (figure 7). Such configurations generate the greatest number of logarithms of Q^2 in the evolution of the structure functions. Sub-leading corrections are classified according to the number of k_t -disordered rungs in the ladder. The HERWIG event generator [18], as well as the matrix element plus parton shower (MEPS) option of LEPTO [29], are implementations of DGLAP evolution, with different approximate treatments of sub-leading terms. The ARIADNE generator [30] uses the colour dipole model (CDM) [31], in which disordered transverse momentum configurations are permitted but the radiated gluons are regarded as emitted by the proton remnant, so the connection with the picture in figure 7 is not so clear.

At very small x , a classification of contributions according to the degree of ordering in x rather than k_t becomes more appropriate, because logarithms of x dominate over those of Q^2 . The most widely used approach is that based on the BFKL equation [32], which describes the x -dependence of the structure function in terms of a sum over ladder graphs that exhibit strong ordering in x without ordering in transverse momentum. The original BFKL derivation was based on multi-Regge dynamics, in which k_t values are limited. More recently, the same equation for the x -dependence of the structure function has been

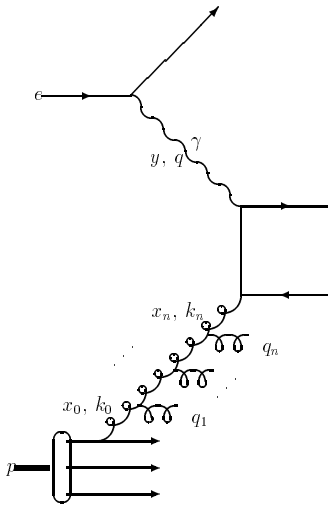


Figure 7. Ladder graph for DIS at small x .

derived by Ciafaloni, Catani, Fiorani and Marchesini (CCFM) [33] from an approach based more closely on QCD, in particular on the coherence properties of the theory at small x . Although the CCFM approach leads to the same equation as BFKL when summed over all final states, it gives a different picture of less inclusive quantities [34].

In order to compare the results of the two approaches, it is convenient to perform a Mellin transformation, introducing the moment variable ω conjugate to x :

$$\tilde{F}(\omega) = \int_0^1 dx x^\omega F(x). \quad (21)$$

Then the objective at small x is to sum to all orders in α_s the terms that are most singular at $\omega = 0$. In both approaches the structure function is expressed as a sum over ladder contributions as in figure 7:

$$\tilde{F}(\omega, Q/\mu) = \sum_{r=0}^{\infty} \tilde{F}^{(r)}(\omega, Q/\mu) \quad (22)$$

where r is the number of rungs in the ladder and μ is an infrared cutoff. In the BFKL case one may write the ladder contributions in the form

$$\tilde{F}_{\text{BFKL}}^{(r)} \sim \int_{q_i=\mu}^Q \prod_{i=1}^r \frac{d^2 q_i}{\pi q_i^2} \frac{dz_i}{z_i} z_i^\omega \bar{\alpha}_s \Delta_{\text{R}}(z_i, k_{ti}), \quad (23)$$

where the variable q_i is related to the transverse momentum q_{ti} and longitudinal momentum fraction $(1 -$

$z_i)$ of an emitted gluon, $q_i = q_{ti}/(1 - z_i)$, $k_{ti} = \sum_{j=1}^i q_{tj}$ is the corresponding exchanged transverse momentum, and $\bar{\alpha}_s = C_A \alpha_s / \pi$. The function $\Delta_{\text{R}}(z_i, k_{ti})$ is a Regge form factor,

$$\Delta_{\text{R}}(z_i, k_{ti}) = \exp \left(-\bar{\alpha}_s \int_{z_i}^1 \frac{dz}{z} \int_{\mu^2}^{k_{ti}^2} \frac{dk_t^2}{k_t^2} \right). \quad (24)$$

The CCFM expression corresponding to eq. (23) is

$$\tilde{F}_{\text{CCFM}}^{(r)} \sim \int_{q_i=0}^Q \prod_{i=1}^r \frac{d^2 q_i}{\pi q_i^2} \frac{dz_i}{z_i} z_i^\omega \bar{\alpha}_s \Delta_{\text{N}}(z_i, k_{ti}, q_i) \times \Theta(q_i - z_{i-1} q_{i-1}) \Theta(q_1 - \mu). \quad (25)$$

The main differences are the ordering condition $q_i > z_{i-1} q_{i-1}$, which corresponds to *angular ordering* of gluon emission due to coherence, and the replacement of the Regge form factor (24) by the ‘non-Sudakov’ form factor

$$\Delta_{\text{N}}(z_i, k_{ti}, q_i) = \exp \left(-\bar{\alpha}_s \int_{z_i}^1 \frac{dz}{z} \int_{z^2 q_i^2}^{k_{ti}^2} \frac{dk_t^2}{k_t^2} \right). \quad (26)$$

This leads to the same asymptotic behaviour for the structure function:

$$\tilde{F}_{\text{BFKL}} \sim \tilde{F}_{\text{CCFM}} \sim 1 + 2\bar{\alpha}_s \frac{t}{\omega} + 2\bar{\alpha}_s^2 \frac{t^2}{\omega^2} + \dots, \quad (27)$$

where $t = \ln(Q/\mu)$. However, the final state properties are different. For example, the mean number of ladder rungs, which gives the mean number of primary emitted gluon jets, is related to the quantity $\sum r \tilde{F}^{(r)}$, for which one finds [34]

$$\begin{aligned} \sum r \tilde{F}_{\text{BFKL}}^{(r)} &\sim 2\bar{\alpha}_s \frac{t}{\omega} + 6\bar{\alpha}_s^2 \frac{t^2}{\omega^2} + \dots \\ \sum r \tilde{F}_{\text{CCFM}}^{(r)} &\sim 2\bar{\alpha}_s \frac{t}{\omega} + 4\bar{\alpha}_s^2 \left(\frac{t^2}{\omega^2} + \frac{t}{\omega^3} \right) + \dots \end{aligned} \quad (28)$$

Notice that the BFKL series for this quantity, like that for the structure function itself, involves at most one extra factor of $1/\omega$ for each power of α_s , whereas the CCFM series contains up to two such factors. The new terms are subleading with respect to the number of logarithms of Q but dominate at small x ($\omega \rightarrow 0$). The corresponding expansions for the mean number of primary emitted jets are

$$\begin{aligned} \langle r \rangle_{\text{BFKL}} &\sim 2\bar{\alpha}_s \ln \frac{Q}{\mu} \left[1 + \bar{\alpha}_s \ln \frac{1}{x} \ln \frac{Q}{\mu} + \mathcal{O}(\alpha_s^3) \right], \\ \langle r \rangle_{\text{CCFM}} &\sim 2\bar{\alpha}_s \ln \frac{Q}{\mu} \left[1 + \bar{\alpha}_s \ln^2 \frac{1}{x} - \frac{1}{6} \bar{\alpha}_s^2 \ln^4 \frac{1}{x} \right. \\ &\quad \left. + \mathcal{O}(\alpha_s^3) \right]. \end{aligned} \quad (29)$$

We see that more emission at small x is predicted by the CCFM treatment. The reason is that the angular

ordering prescription in eq. (25) corresponds to an increased phase space compared to that available in eq. (23) for any fixed value of the infrared cutoff μ .

So far, the CCFM approach has not reached the stage of detailed phenomenological application, and so the quantitative differences between the CCFM and BFKL predictions for final states in the accessible domain of x and Q^2 are not yet clear. Predictions of CCFM and DGLAP evolution were compared in ref. [35] at large Q^2 down to $x \sim 10^{-5}$ and the differences were not great; one would expect CCFM and BFKL to be even more similar.

3.2. Transverse energy flow

The new basic feature of small- x physics (in both the BFKL and CCFM formulations) is the loss of strong ordering of exchanged and emitted transverse momenta. This suggests that one should see extra transverse energy emission in small- x events, especially in the region well separated from both the current and remnant jets. The HERA experiments do see a substantial transverse energy per unit rapidity in this region (about 2 GeV per unit rapidity) [36, 37, 38], with some indication of a rise at small x , as shown for example by the H1 data in figure 8. The curves show that standard DGLAP evolution as implemented in the MEPS model (defined above) does not produce such a rise, while the colour dipole model and a BFKL-based calculation [39] do, presumably because of their inclusion of k_t -disordered contributions.

One point to bear in mind when comparing theoretical predictions for transverse energy flow is that they are highly sensitive to the correct treatment of the hard scattering process that takes place at the top of the ladder in figure 7. This is because the mean emitted transverse energy is obtained by inserting a factor of k_{ti} into the integration in eq. (23) or (25). As a result, the integral becomes more sensitive to the region $k_{ti} \sim Q$. In the case of the DGLAP evolution equation, which assumes strong ordering in k_t , the k_t -ordering above the i -th rung is in fact destroyed by inserting a factor of k_{ti} , and so the relevance of the equation becomes questionable. Preferably, one should compute the transverse energy emission at a particular rapidity from the full hard scattering matrix elements for producing additional partons in that direction.

An illustration of the above point was provided by the HERWIG (version 5.7 and earlier) prediction for the transverse energy flow, which had a deficit in the rapidity range of interest. This was because the parton shower approximation to the hard matrix elements (with the choice of evolution variables used in HERWIG) left a region of phase space unpopulated by emitted partons. In version 5.8 a matrix element correction was included

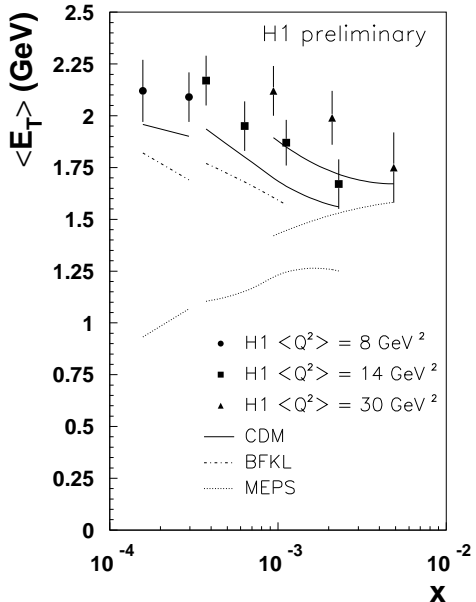


Figure 8. Mean transverse energy flow per unit rapidity (at zero rapidity in the hadronic c.m. frame), as a function of Bjorken x , for various ranges of Q^2 .

and the transverse energy flow became consistent with the data, without any retuning of parameters [40].

3.3. Associated forward jets

The most reliable indicator of new physics at small x still seems to be the associated production of jets in the forward (proton) direction with relatively large momentum fractions x_{jet} and transverse momenta $q_{t,jet} \sim Q$ [41]. In this region there is no phase space for DGLAP evolution with transverse momentum ordering, whereas the scope for BFKL evolution in x remains large. Thus a strong increase in production of such jets is expected with decreasing Bjorken x [42]. Since the cross section is fully inclusive with respect to what lies between the forward and current jets, the CCFM approach leads to the same conclusion.

The H1 data (figure 9) [37] do indeed show a high event rate at small x . The data shown are for events at $Q^2 \sim 20$ GeV 2 with jets with $x_{jet} > 0.025$, $0.5 < q_{t,jet}^2/Q^2 < 4$ and $q_{t,jet} > 5$ GeV. The predictions of the colour dipole and MEPS models are also shown. While the colour dipole model does show a rise at small x , it predicts an even lower rate than MEPS if the cut on x_{jet} is increased to 0.05 [37].

At present the lack of a full BFKL-based event generator prevents a comparison with the BFKL prediction including selection cuts and detector and hadronization corrections. However, a parton-level BFKL calculation [42] predicts a ratio of about 1.6

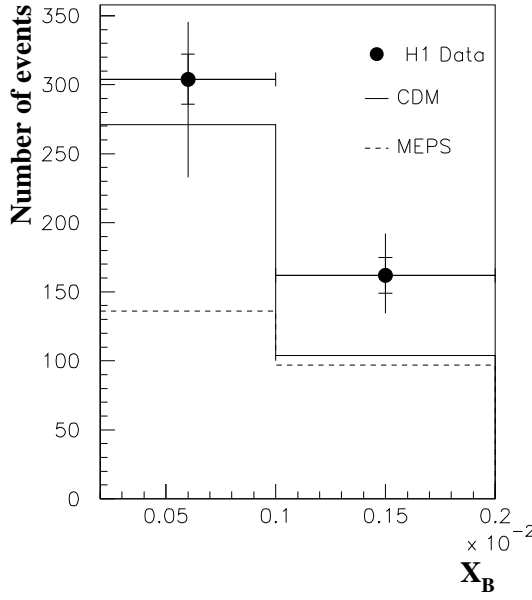


Figure 9. Forward jet production rate as a function of Bjorken x .

between the two x bins in figure 9, which is consistent with the data.

4. Exotic QCD

4.1. Instanton-induced processes

An intriguing possibility raised in recent theoretical papers [43, 44, 45], but not so far subjected to experimental investigation, is that fundamentally non-perturbative features of QCD may lead to exotic new processes in DIS. Such processes can arise from the structure of the QCD vacuum, which contains topologically non-trivial gauge field configurations characterized by an integer value of a quantity called the Chern-Simons number, N_{CS} . Configurations with adjacent values of N_{CS} are separated by an energy barrier. The process of tunnelling through this barrier is represented by a space-time configuration called an *instanton* [46].

An important feature of the instanton tunnelling process is that the change in the gauge field induces a change in the fermion sector of the theory. In the case of QCD the fermionic change involves the axial charge Q_5 :

$$\Delta Q_5 = 2\Delta N_{\text{CS}} = 2N_f \quad (30)$$

where N_f is the number of active flavours. Since the axial charge measures the chirality or handedness of the fermions, this implies that the process is chirality-violating. In electroweak interactions the effect is more

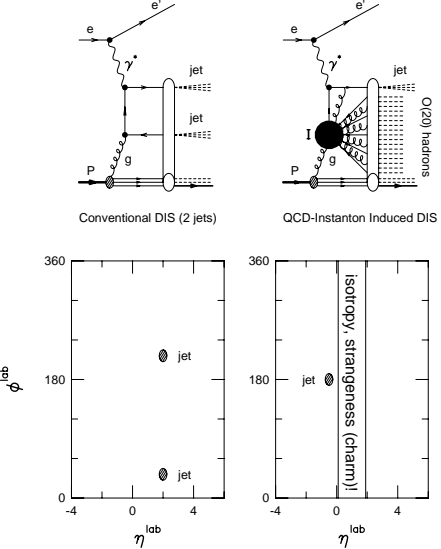


Figure 10. Comparison between conventional and instanton-induced DIS events.

spectacular: the tunnelling process leads to violation of baryon- and lepton-number conservation [46]. Thus it is possible (though at present considered unlikely) that instanton-induced processes could be responsible for the net baryon number of the universe. This makes it all the more interesting to look for the analogous processes in QCD, which turn out to have much larger predicted cross sections, essential because $\alpha_s \sim 1/8$ is much larger than $\alpha_w \sim 1/30$. (For a tunnelling process, a factor of $1/\alpha$ appears in the exponent of the transition rate - see eq. (32) below.)

Taking $N_f = 3$, eq. (30) implies that processes like

$$\gamma^* \rightarrow u_L \bar{u}_R, \bar{u}_R + g \rightarrow \bar{u}_L u_L d_L s_L \bar{u}_L \bar{d}_L \bar{s}_L + \text{gluons} \quad (31)$$

can occur (figure 10). The subscripts indicate that the outgoing quarks and antiquarks are all left-handed. The chirality violation would be difficult to observe experimentally, but the relatively high multiplicity, including excess strange (possibly even charmed) particle production, should be characteristic. The typical number of gluons produced is expected to be of order $\pi/2\alpha_s \sim 10$, further enhancing the multiplicity. Another distinctive feature is the relative isotropy of the final state in the rest-frame of the instanton subprocess, which transforms into a band about two units wide in the lab rapidity distribution, in contrast to the more normal jet-like configurations, as indicated in the lower half of figure 10.

A Monte Carlo generator for such events is under development [47]: a typical simulated event is depicted

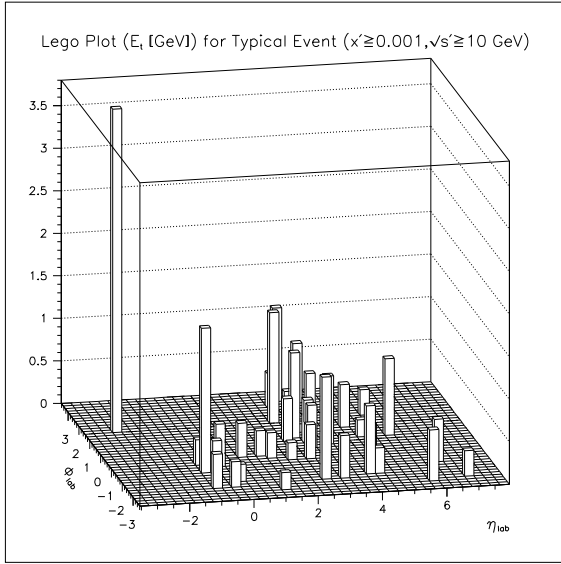


Figure 11. ‘Lego plot’ for simulated QCD instanton-induced event.

in figure 11. The isolated particle at $\eta_{\text{lab}} \simeq -2.5$ is the electron, while the current-quark jet is around $\eta_{\text{lab}} \simeq -0.5$. The densely populated band at $\eta_{\text{lab}} \simeq 2-4$ is the final state from the instanton-induced process.

A general difficulty with instanton-induced processes is that they are normally suppressed by large inverse powers of Q^2 . The cross section is of the form

$$\sigma(x', Q'^2) \sim \frac{1}{s'} \exp \left\{ -\frac{4\pi}{\alpha_s(Q')} S(x') \right\} \quad (32)$$

where s', x', Q' are the c.m. energy squared and Bjorken variables of the instanton subprocess (the blob I in figure 10). $S(x')$ is an increasing function, approaching unity at large x' but unfortunately not yet calculable at small x' . This translates into a contribution to the structure function F_2 as shown in figure 12. The dashed curves are contours of constant S . The region labelled “data” corresponds roughly to the trend of the experimental data on F_2 . Thus at $x < 0.3$ a detectable signal could be present, if S becomes small enough.

5. Conclusions

Both experimental and theoretical studies of DIS final states are still in their infancy. Although things are not so simple as in e^+e^- annihilation, because of the presence of the incoming proton and its outgoing remnant, DIS has the advantage of covering a wide range of Q^2 at a single beam energy. This is already leading to evidence for the running of α_s from multi-

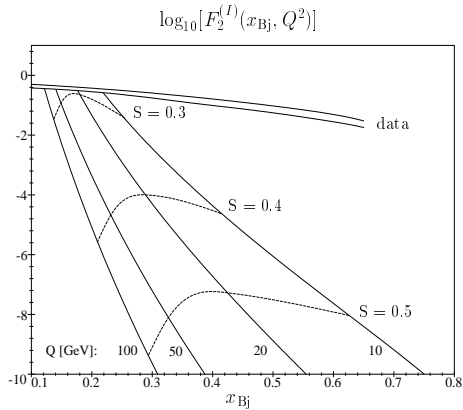


Figure 12. Logarithm of the instanton-induced contribution to the structure function F_2 of the proton.

jet production rates; we can expect similar results from analyses of event shapes and jet fragmentation, plus a host of new data on power-suppressed corrections, which will improve understanding of the interface between perturbative and non-perturbative QCD. In the small- x region, theoretical ideas and experimental data on final state properties could be crucial in elucidating the mechanism that causes the rise in the structure function F_2 . A search for exotic final states due to instanton-induced processes could shed new light on non-perturbative QCD, and might establish the credibility of analogous electroweak processes as a source of baryon- and lepton-number violation within the Standard Model.

Acknowledgement

It is a pleasure to thank Violette Brisson and the committee for organizing this most stimulating workshop.

References

- [1] D. Graudenz, Phys. Lett. B256 (1991) 518; Phys. Rev. D49 (1994) 3291;
- T. Brodkorb and J.G. Körner, Z. Phys. C54 (1992) 519;
- T. Brodkorb and E. Mirkes, Z. Phys. C66 (1995) 141.

[2] JADE collaboration, W. Bartel et al., *Z. Phys. C33* (1986) 23.

[3] H1 collaboration, T. Ahmed et al., *Phys. Lett. B346* (1995) 415.

[4] ZEUS collaboration, M. Derrick et al., preprint DESY 95-182 (hep-ex/9510001).

[5] B.R. Webber, *J. Phys. G* 19 (1993) 1567.

[6] S. Catani, Yu.L. Dokshitzer and B.R. Webber, *Phys. Lett. B285* (1992) 291.

[7] E. Farhi, *Phys. Rev. Lett.* 39 (1977) 1587.

[8] B.R. Webber, *Phys. Lett. B339* (1994) 148; see also *Proc. Summer School on Hadronic Aspects of Collider Physics, Zuoz, Switzerland, August 1994*, ed. M.P. Locher (PSI, Villigen, 1994).

[9] H. Contopanagos and G. Sterman, *Nucl. Phys. B419* (1994) 77; G.P. Korchemsky and G. Sterman, *Nucl. Phys. B437* (1995) 415;

[10] A.V. Manohar and M.B. Wise, *Phys. Lett. B344* (1995) 407;

[11] Yu.L. Dokshitzer and B.R. Webber, *Phys. Lett. B352* (1995) 451.

[12] R. Akhoury and V.I. Zakharov, *Phys. Lett. B357* (1995) 646.

[13] P. Nason and M.H. Seymour, preprint CERN TH/95-150 (hep-ph/9506317).

[14] M. Beneke and V.M. Braun, preprint DESY 95-120 (hep-ph/9506452).

[15] Yu.L. Dokshitzer, G. Marchesini and B.R. Webber, CERN preprint in preparation.

[16] S. Catani, Yu.L. Dokshitzer and B.R. Webber, in preparation.

[17] T. Sjöstrand, *Comp. Phys. Comm.* 39 (1986) 347;
T. Sjöstrand and M. Bengtsson, *Comp. Phys. Comm.* 43 (1987) 367.

[18] G. Marchesini, B.R. Webber, G. Abbiendi, I.G. Knowles, M.H. Seymour and L. Stanco, *Comp. Phys. Comm.* 67 (1992) 465.

[19] Yu.L. Dokshitzer, D.I. Dyakonov and S.I. Troyan, *Phys. Reports* 58 (1980) 270;
D. Amati, A. Bassetto, M. Ciafaloni, G. Marchesini and G. Veneziano, *Nucl. Phys. B173* (1980) 429.

[20] A.H. Mueller, in *QCD 20 Years Later*, vol. 1 (World Scientific, Singapore, 1993).

[21] S. Catani, G. Turnock and B.R. Webber, *Phys. Lett. B295* (1992) 269.

[22] H1 collaboration, S. Aid et al., *Nucl. Phys. B445* (1995) 3.

[23] ZEUS collaboration, M. Derrick et al., *Z. Phys. C67* (1995) 93.

[24] A.H. Mueller, *Phys. Lett. B104* (1981) 161; *Nucl. Phys. B213* (1983) 85.

[25] E.D. Malaza and B.R. Webber, *Nucl. Phys. B267* (1986) 702.

[26] C.P. Fong and B.R. Webber, *Nucl. Phys. B355* (1991) 54.

[27] W.J. Stirling, these proceedings.

[28] Yu. L. Dokshitzer, *Sov. Phys. JETP* 46 (1977) 641;
V.N. Gribov and L.N. Lipatov, *Sov. J. Nucl. Phys.* 15 (1972) 438, 675;
G. Altarelli and G. Parisi, *Nucl. Phys.* 126 (1977) 297.

[29] G. Ingelman, in *Proc. Workshop on Physics at HERA, Hamburg, 1991*, vol. 3, ed. W. Buchmüller and G. Ingelman (DESY, Hamburg, 1992).

[30] L. Lönnblad, *Comp. Phys. Comm.* 71 (1992) 15.

[31] B. Andersson, G. Gustafson, L. Lönnblad and U. Pettersson, *Z. Phys. C43* (1989) 625.

[32] E.A. Kuraev, L.N. Lipatov and V.S. Fadin, *Sov. Phys. JETP* 45 (1972) 199;
Y.Y. Balitsky and L.N. Lipatov, *Sov. J. Nucl. Phys.* 28 (1978) 282.

[33] M. Ciafaloni, *Nucl. Phys. B296* (1988) 49;
S. Catani, F. Fiorani and G. Marchesini, *Phys. Lett. B234* (1990) 339; *Nucl. Phys. B336* (1990) 18.

[34] G. Marchesini, *Nucl. Phys. B445* (1995) 49.

[35] G. Marchesini and B.R. Webber, *Nucl. Phys. B349* (1991) 617.

[36] H1 collaboration, I. Abt et al., *Z. Phys. C63* (1994) 377.

[37] H1 collaboration, S. Aid et al., *Phys. Lett. B356* (1995) 118.

[38] T. Haas, these proceedings.

[39] J. Kwieciński, A.D. Martin, P.J. Sutton and K. Golec-Biernat, *Phys. Rev. D50* (1994) 217;
K. Golec-Biernat, J. Kwieciński, A.D. Martin and P.J. Sutton, *Phys. Lett. B335* (1994) 220.

[40] M.H. Seymour, *Nucl. Phys. B436* (1995) 443; Lund preprint LU-TP-94-12 (1994).

[41] A.H. Mueller, *Nucl. Phys. B* (Proc. Suppl.) 18C (1990) 125; *J. Phys. G17* (1991) 1443.

[42] J. Kwieciński, A.D. Martin, P.J. Sutton, *Phys. Rev. D46* (1992) 921.

[43] I. Balitsky and V. Braun, *Phys. Lett. B314* (1993) 237.

[44] A. Ringwald and F. Schrempp, preprint DESY 94-197, to be published in *Proc. Quarks-94*, Vladimir, Russia (hep-ph/9411217).

[45] M. Gibbs, A. Ringwald and F. Schrempp, preprint DESY 95-119 (hep-ph/9506392).

[46] G. 't Hooft, *Phys. Rev. Lett.* 37 (1976) 8, *Phys. Rev. D14* (1976) 3432;
A. Belavin, A. Polyakov, A. Schwarz and Yu. Tyupkin, *Phys. Lett. B59* (1975) 85;
A. Ringwald, *Nucl. Phys. B330* (1990) 1;
O. Espinosa, *Nucl. Phys. B343* (1990) 310

[47] M. Gibbs, A. Ringwald and F. Schrempp, work in progress.